Miniature Ferroelectret Microphone Design and Performance Evaluation Using Laser Excitation

Linas Svilainis, Andrius Chaziachmetovas, Valdas Eidukynas, Tomás Gómez Álvarez-Arenas and Steve Dixon

***Abstract*—Miniature microphones suitable for measurements of ultrasonic wave field scans in air are expensive, or lack sensitivity or do not cover the range beyond 100 kHz. Essential, that they are too large for such fields measurements. The use of ferroelectret (FE) film is proposed to construct a miniature, needle-style 0.5 mm diameter sensitive element ultrasonic microphone. FE has an acoustic impedance much closer to that of air compared to other alternatives, and is low cost and easy to process. Performance of the microphone was evaluated by measuring the sensitivity area map, directivity, AC response and calibrating the absolute sensitivity. Another novel contribution here, is that the sensitivity map was obtained by scanning the focused beam of a laser diode over the microphone surface, producing thermoelastic ultrasound excitation. The electroacoustic response of the microphone served as a sensitivity indicator at a scan spot. Micrometer scale granularity of the FE sensitivity was revealed in the sensitivity map images. It was also demonstrated that the relative AC response of the microphone can be obtained using pulsed laser beam thermoelastic excitation of the whole microphone surface with a laser diode. The absolute sensitivity calibration was done using the hybrid three transducer reciprocity technique. A large aperture, air coupled transducer beam was focused onto the microphone surface, using the parabolic off-axis mirror. This measurement validated the laser AC response measurements. FE microphone performance was compared to bi-axially stretched PVDF (Polyvinylidene difluoride) microphone of the same construction.**

***Index Terms*—air coupled ultrasound, ferroelectret film, laser ultrasound, ultrasonic needle microphone.**

I. Introduction

MANY applications, like local positioning systems, ranging, obstacle avoidance, anemometry or non-destructive testing utilize air-coupled ultrasound. Air-coupled ultrasound applications call for efficient signal transduction, due to the high acoustic impedance mismatch between air and the samples of interests. Therefore, most effort is usually concentrated on transducer development. A necessary measurement in transducer development is the directivity and acoustic field distribution [1]-[11]. A ball reflector is used for such measurements, if only the pulse-echo directivity is required [5],[6]. A small size receiver is used for the field distribution measurements. The size of the sensing element of the receiver should be less than the wavelength of twice the central frequency of the probe under test, but not less than 0.5 mm [6]. However, there are no ultrasonic range microphones of this size available. The most frequently used type of microphone is the 1/8" (3.18 mm diameter) type 4138 microphone from Brüel & Kjær (Nærum, Denmark) [2]-[4],[10],[11]. Unfortunately, its bandwidth is limited to 140 kHz [1], and its relatively large size means that it is only really useful up to 50 kHz, if spatial averaging effects are to be avoided [6]-[9]. Most microphones are intended for applications that are not required to go beyond 100 kHz. In addition, sensitivity decreases with the frequency, and it is often difficult to avoid the appearance of resonances that destroy the expected flat response of the microphone. These include resonances in the structure of the microphone and even resonances in the sensing material. Another alternative microphone design is the PVDF (Polyvinylidene difluoride) membrane hydrophone, whose active area diameter can be down to 0.5 mm [12]. It has a wide, uniform frequency response from 100 kHz up to 5 MHz, but the device diameter including the frame is 60 mm. The PVDF membrane also has to be perforated around the sensing area, in order to avoid Lamb wave generation on the membrane. Another widely used alternative is the miniature piezoceramic disk "pinducer" [3],[4] (for example the VP-1093 from the Valpey -Fisher Corporation), which has a diameter of 1.35 mm. Though the acoustic impedance of the PVDF membrane is an order of magnitude lower than the piezoceramic in the pinducer, the pinducer is often preferable given its greater piezoelectric sensitivity and improved directional response. PVDF needle hydrophones, despite being intended for use in water, can also be considered, but as with pinducers they have a large impedance mismatch to air, so that sensitivity for a 0.5 mm hydrophone is 0.8 μV/Pa [59]. Placing an aperture in front of the receiver can attain a 1 mm diameter sensing area [13], but the parasitic capacitance remains high, so sensitivity is low. Optical ultrasound microphones can be divided into four categories: i) the Fabry-Perot resonator [15] at the end of an optical fiber; ii) the distributed Bragg reflector (DBR) [16],[25] at the end of the optical fiber iii) the ring resonator coupled to

This work was supported by European Regional Development Fund (project No. 01.2.2-LMT-K-718-03-0026) under grant agreement with the Research Council of Lithuania (LMTLT). *(Corresponding author: L. Svilainis).*

L. Svilainis and A. Chaziachmetovas are with the Electronics Engineering Department, Kaunas University of Technology, Kaunas, LT-51368 Lithuania (e-mail: linas.svilainis@ktu.lt; andrius.chaziachmetovas@ktu.lt).

V. Eidukynas is with the Department of Mechanical Engineering and Design, Kaunas University of Technology, Kaunas, LT-51368 Lithuania (e-mail: valdas.eidukynas@ktu.lt).

Tomás Gómez Álvarez-Arenas is with the Institute for Physical and Information Technologies, Spanish National Research Council, 28006 Madrid, Spain (e-mail: t.gomez@csic.es).

Steve Dixon is with the Department of Physics, University of Warwick, Coventry CV4 7AL, U.K. (e-mail: s.m.dixon@warwick.ac.uk).

the optical fiber or waveguide [14],[24] and iv) refraction index modulation-based sensors [18]-[20]. The interferometric cavity microphone (based on refraction index modulation) commercially available from XARION Laser Acoustics has a sensing aperture of 2.0 mm x 0.3 mm [18]. Another simple approach is to use a pellicle and laser vibrometer to detect displacement of the pellicle [58]. While offering wide bandwidth and a small sensitive area size (e.g. Fabry-Perot interferometer-based FOHSv2, commercially available from Precision Acoustics Ltd [17]), this type of sensor requires an additional light-processing engine, and the whole system can be expensive. Micromachined (MEMS) air-coupled ultrasonic sensors [21]-[23], [26], [27] can have sensitive element sizes of 0.1 mm [21]. The appearance of novel applications in the field of consumer electronics and the use of MEMS microphones [23] is extending this range up to 200 kHz. Although it is crucial for the study of higher frequency ultrasonic air-coupled ultrasonic transducers used in NDT, there is still little interest in these novel applications for further increasing this frequency range. Finally, MEMS devices need intricate chip fabrication technology and their structure can be extremely fragile. Commercially available MEMS based microphones can operate up to frequencies of 80 kHz [39].

To conclude, there are no suitable, inexpensive, microphones less than 3 mm diameter available for ad-hoc measurements and scans of ultrasonic fields in air. The current options that are available, are either expensive (optical microphones are 10k USD order, hydrophones 1k USD), or lack sensitivity due to an impedance mismatch to air, or are large or do not cover the frequency range beyond 100 kHz. The key challenges are the size (0.5 mm diameter), sensitivity and cost.

The ferroelectret (FE) is one of the recently proposed materials for ultrasound transmission and detection [28]-[34]. While the piezoelectric strain constant d_{33} for PVDF is around 20 pC/N, d_{33} for FE devices range from 25 pC/N to 700 pC/N, with new developments reaching 1200 pC/N [34] or even 1400 pC/N [35]. FE devices have a lower density, of around (330-530) kg/m^3, and a lower speed of sound in the material of 85-177 m/s, resulting in an acoustic impedance that is much closer to that of air when compared to other alternatives, (0.028-0.056) MRayl [31]-[33]. The FE material is low cost, is readily commercially available and usually comes with one side metalized. It is bonded to a rigid backing so that it operates by compressing in its thickness direction, rather than via a flexing mechanism. The properties of the FE material can also be further improved by additional processing [38]. There have been reports [36],[37] of applications using FE sensors, but of 5x5 mm size, with a sensitivity of 2 mV/Pa and bandwidth of only 10 kHz.

Here we report the design and of a small, 0.5 mm diameter, FE-based microphone, operating in the 150-450 kHz frequency range. Construction is very simple and mainly involves adhesively bonding the FE film onto the end of the semirigid coaxial cable. Material and labor cost is minimal. A similar construction of microphone was produced using PVDF, for comparison purposes. The sensitive area size was measured using focused laser ultrasound with μm resolution. Absolute sensitivity and AC response were measured in the 150 kHz to 450 kHz frequency range, using a hybrid three transducer reciprocity technique [59]. Relative AC response was measured using wide beam laser ultrasound.

II. Microphone Design

A schematic diagram of the FE microphone's construction and a photograph of the assembled device are presented in Fig.1. The 70 μm thick EMFIT film HS-03-20BRAL1 (from EMFIT. Ltd., Vaajakoski, Finland) was used in this microphone design. The film was adhesively bonded (using MB295 from Master Bond, Hackensack, NJ, US) onto the end of 15 mm long, 2.159 mm diameter, RG405 type, semirigid coaxial cable (from Belden, Inc., St. Louis, MO, US). The other end of the semirigid cable was soldered into an SMA connector (2911-40024 type, from Amphenol, Wallingford, CT, US). The EMFIT film comes with one side already metalized, which faced outwards and served as ground electrical connection. Connection to the cable shield was made using silver conductive paint (SCP03B from Electrolube, Leicestershire, UK). The center conductor (0.5 mm diameter) of the coaxial cable served as the "live" electrode for the FE film.

Fig. 1. Microphone construction (left) and the assembled device (right).

The output of the microphone was directly connected to a 40 dB preamplifier (SE-RX01-02), that was designed and manufactured by Kaunas University of Technology (KTU). The preamplifier input impedance was 5 kΩ, the lower passband frequency was 90 kHz, with an additional third order Butterworth filter limiting the upper passband frequency to 3 MHz. More details on the preamplifier design and noise performance can be found in [41].

The PVDF-based hydrophone was manufactured using the same construction as the FE microphone. A bi-axially stretched 50 μm thick PVDF film (from Piezotech Arkema-CRRA, Pierre-Benite Cedex, France) was used. The PVDF film was supplied with metallization on both sides, so one electrode was etched out.

In both cases, PVDF and FE, the vibrational mode of the sensor is the thickness mode, and thickness is much smaller than the lateral dimension. Moreover, in the case of the FE material, the large anisotropy grants a large decoupling between thickness and lateral vibration modes. The microscopic scale simulation, presented in [28] confirms that simple thickness resonance calculation is sufficient for AC response estimation. Material properties (thickness h, density ρ, propagation velocity c, quasi-static piezoelectric coefficient d_{33}) and the expected $\lambda/4$

resonance frequency (the backing is copper, high impedance) are listed in Table I.

TABLE I
PROPERTIES OF FE FILM USED FOR MICROPHONE DESIGN

Material	h, µm	ρ, kg/m^3	$f_{rez\lambda/4}$,MHz	c, m/s	d_{33}, pC/N
FE	70	530	0.32	90	80
PVDF	40	1780	14	2200	25

The bandwidth used in the investigation was set to 150 kHz-450 kHz (+/-50% f_{rez}), which was limited by the resonance frequency of the FE microphone.

III. PERFORMANCE EVALUATION

The size of the "live" electrode (0.5 mm diameter center conductor of the coaxial cable) is intended to define the size of the sensitive area of the microphone. Nevertheless, experiments were set to evaluate the active area size of the microphone, as pressure waves incident to the side of the central reason could in principle yield a response.

A. Sensitive Area Size Evaluation Using Laser Ultrasound

The evaluation of the size of the sensitive area size can be performed using a focused transducer, scanning over the probe's surface [42],[43]. However, the focused probe's beam should be 50 µm diameter or smaller, in order to scan the 0.5 mm diameter area. Focusing an air-coupled ultrasonic transducer to such a small size would be challenging, not least because the ultrasonic wavelength is almost 2.2 mm at 150 kHz. A reasonable alternative approach seems to be using a laser ultrasound source [44], which can be directly coupled to the surface of the test sample. The acoustic contact is stable, there is no need for immersion, impedance mismatch does not affect the signal level and there is no reverberation in the coupling media. It can also be focused to a small size, with a laser spot of 50 µm diameter being attainable. It is important, that such a source is not resonant, and the pulsed laser beam can provide wideband excitation with an arbitrary source shape, using suitable optics [45].

The thermoelastic regime (power density below the damage threshold of the test material) [46] was used. In this case the thermal expansion of the volume heated by laser pulse is the major source of the ultrasound.

Pulsed laser diodes are now commercially available at a reasonable cost, and the planned application will send series of pulses. The laser drivers required to do this are not currently commercially available, but the development of such a laser driver has been reported [48]. However, the laser diode used in [48] has a highly asymmetric beam shape: the laser aperture size is 225x10 µm. This is an inherent property of >10 W laser diodes, because they are edge-emitting devices. The 10 µm dimension is too small, and a large portion of acoustic energy is converted into other modes and only a small amount is directed normal to the surface. The 225 µm dimension is really too wide to scan an area of 500 µm diameter. Therefore, a different laser diode type, with an aperture size of 85x10 µm was used (905D1S3J03UA type, 27 W at 11 A from Laser Components, Olching, Germany).

However, the above mentioned modification was not sufficient for scanning requirements: the beam shape at focus was still asymmetric, and edge-emitting lasers also have inherent astigmatism [51],[52] (virtual emission origin for slow and fast axis do not match). Usually, a dedicated lens system is designed to solve this issue [51]-[53], or a complex optical system including cylindrical lenses [54] or a pair of anamorphic prisms is used [55]. The case presented here used a simpler approach: instead of correcting the astigmatism, it was exploited. Due to astigmatism, when the fast axis is focused, the slow axis is slightly defocused, so it is blurred. But 250 µm further from the laser from this focus point, the slow axis gets focused, and the fast axis starts to be blurred (Fig.2, Fig.3), which yields a symmetric beam shape at this point.

The laser beam can be made smaller using different lens combinations, but a smaller beam has a lower portion of pressure directed normal to the surface [45]-[47]. Then, in order to have an acceptable acoustic output, laser power has to be increased and the sample surface is potentially damaged due to the increased power density of the beam.

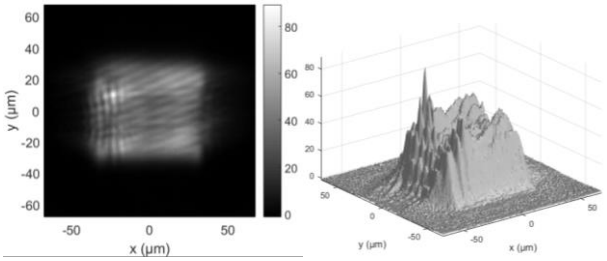

Fig. 2. Laser beam profile in 2D (left) and 3D (right) 250 µm away from focus.

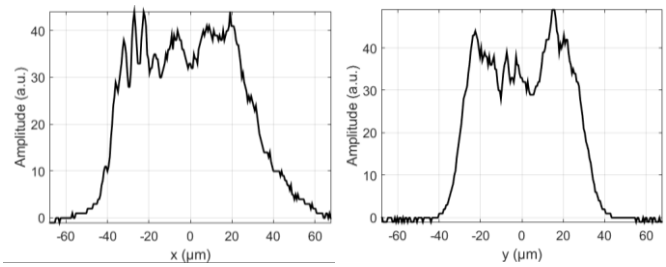

Fig. 3. Beam profile along x (left) and y (right) 250 µm further from focus.

A larger beam size also has a lower power density, so that the danger of ablative surface damage is reduced. A beam size 60x60 µm was found to be optimal, for a balance between resolution and acoustic output. A simple two identical lens (3.1 mm effective focal length, 354330-B type, Thorlabs Inc., NJ, US) 1:1 magnification system was sufficient to focus the laser beam onto the sample surface. The whole laser excitation system (Fig.4: laser driver with current monitor, lens system and encapsulation) design is quite compact, at 40x40x25 mm.

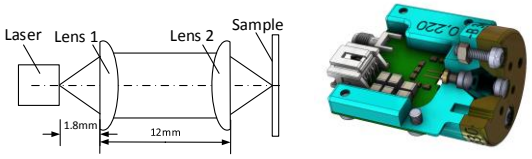

Fig. 4. Lens system (left) and assembled laser probe (right) drawing.

It is easy to position the beam on the sample surface along the z axis: there is a dip in the acoustic response (see Fig.5). The dip occurs due to the narrow laser beam: focusing creates the point-like source and there is less pressure produced normal to the surface [45]-[47].

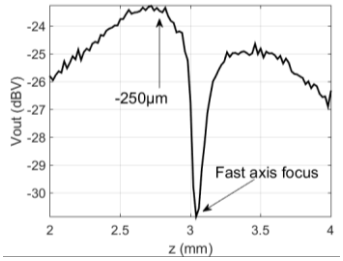

Fig. 5. Acoustic signal intensity versus distance from lens.

The amplitude of the acoustic pressure produced is proportional to the energy absorbed from the laser beam [47]. The microphone's outer surface has an aluminum coating (Fig.1), which reflects a large portion of incident laser energy.

Another problem is that the thermoelastic regime laser ultrasound is plagued by the production of a dual acoustic pulse: a laser generated heat pulse produces two acoustic pulses traveling in opposite directions: towards the material bulk and outwards [49]. The second pulse is immediately reflected back into the material and, if laser penetration depth is small, it cancels the first one. Therefore, generation of the longitudinal waves normal to the material surface is complicated in the thermoelastic regime. However, there is a solution: if a second pulse is either delayed or cancelled, the longitudinal wave normal to the surface is enhanced by several orders of magnitude [46]-[49]. The application of a thin laser energy absorbing layer provides a similar result [60]-[62]. Therefore, the microphone surface was spray-coated with a high temperature paint (800C° BOKSC263206 type from Bostik SA, Colombes, France). The presence of the coating also improves the acoustic pressure produced, due to improved energy absorption and it also reduces the amplitude of the surface wave [50],[63]. Two thicknesses of the coating layer were used: thin (single, brief spray, microphones EMFIT-M1 and PVDF), and thick (two, long sprays, microphone EMFIT-P). One would expect that the thick coating had better absorption, but any additional mass on the EMFIT material will alter its acoustic properties. Thin coating should have less influence.

The laser probe was mounted on a kinematic tilt stage and was attached to a 3D positioning system [57]. The laser was driven by 300 kHz, 5 period, rectangular current tonebursts of 2 A. Such current corresponds to 5 W laser output pulse trains. Adjustment along the z axis was done at a reduced, 1 A current. An example of the received voltage response to laser excitation for the FE and PVDF-based microphone is presented in Fig.6.

An in-house designed ultrasonic data acquisition system was used to drive the laser probe (100 MHz sampling frequency binary coded sets), to digitize the preamplifier output (10-bit, 100 MHz sampling frequency) and to control the 3D positioning (10 µm resolution for x and y axes, and 5 µm resolution for the z axis) [57].

The amplitude and phase of the received signal were estimated using the Sine Wave Correlation (SWC) technique [56]. SWC can be interpreted as a continuous time Fourier transform at single frequency, or as a lock-in amplifier. Thanks to its narrow bandwidth, it can deliver high SNR, and is immune to front ringing caused by the signal's rectangular envelope. The signal was gated by selecting the part of the signal where envelope has reached half of its maximum.

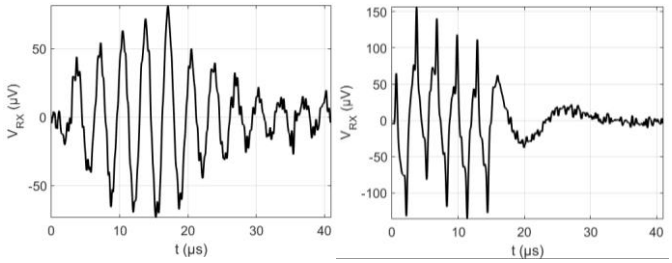

Fig. 6. FE (left) and PVDF-based (right) microphone response to laser excitation.

The C-scan image of the 1200x1200 µm scan over the FE microphone surface with a thin coating at a 10 µm step, is presented in Fig.7 (left: amplitude, right: phase as delay). Phase information was used to gate out the surface waves (equivalent to a 400 ns wide gate placed at 400 ns delay). The corresponding beam profile cross-section is shown in Fig.8.

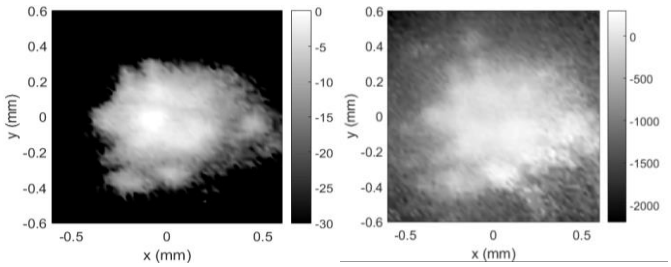

Fig. 7. C-scan of signal amplitude (left, grey scale is dB) and phase (right, grey scale is ns) of microphone EMFIT-M1 (thin light-absorbing coating).

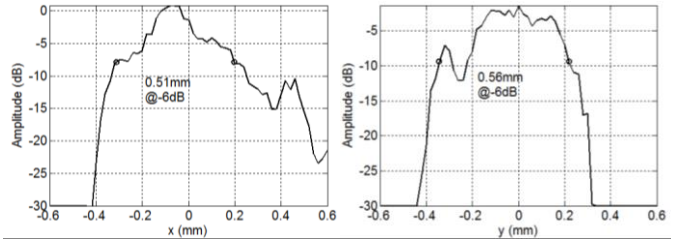

Fig. 8. Beam profile cross-section along x (left) and y (right) axis for microphone EMFIT-M1 (thin light-absorbing coating).

The -6dB sizing approach was used for sensitive area size estimation. The sensitive area size of the EMFIT-M1 microphone is 0.51 mm x 0.56 mm, which is slightly wider than electrode diameter of 0.5 mm. It should be noted that the sensitivity map of this microphone is nonuniform. This is expected, since the FE film contains voids with trapped charge, the lateral size of which varies from few to hundreds of µm [32].

The sensitivity map of the FE microphone with the thick coating is presented in Fig.9, and the corresponding beam

profile cross-section is shown in Fig.10.

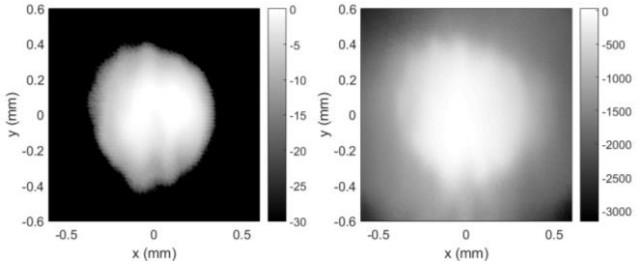

Fig. 9. C-scan of signal amplitude (left, grey scale is dB) and phase (right, grey scale is ns) of microphone EMFIT-P (thick light-absorbing coating).

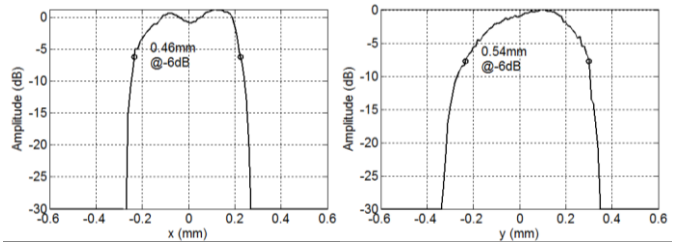

Fig. 10. Beam profile cross-section along x (left) and y (right) axis for microphone EMFIT-P (thick light-absorbing coating).

The thick coating added some smoothing, and the beam profile is more uniform here. The beam size is larger than expected: 0.46 mm x 0.54 mm. Again, phase information was used to gate out the surface waves, which arrive later.

The sensitivity map of the PVDF-based microphone with the thin absorbing coating is presented in Fig.11, and the corresponding beam profile cross-section is shown in Fig.12.

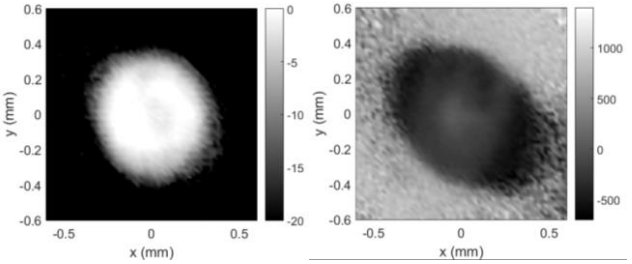

Fig. 11. C-scan of signal amplitude (left, grey scale is dB) and phase (right, grey scale is ns) of PFDV microphone (thin light-absorbing coating).

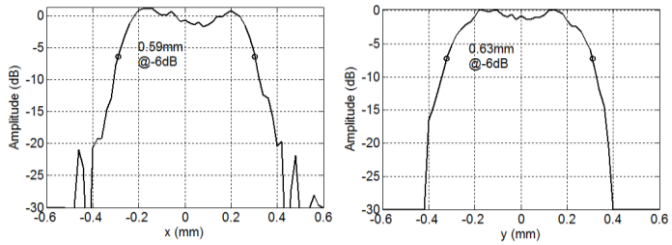

Fig. 12. Beam profile cross-section along x (left) and y (right) axis for PFDV microphone (thin light-absorbing coating).

The sensitivity map of the PVDF version of the microphone is very smooth, with well-defined edges. PVDF material is uniform, so the sensitivity map is uniform too. The beam size is larger than expected: 0.59 mm x 0.63 mm, instead of the expected 0.5 mm diameter of the electrode.

B. Sensitive Area Size Evaluation Using Directivity

Evaluation of the sensitive area size is usually done using a directivity measurement of the hydrophone microphone [64]. Such a measurement is not possible in this case: measurement should be done in the far field, and as the transducer has large aperture, the distance should be large, 200 mm [68]. Air nonlinearity [66] and attenuation effects will be very strong.

Nevertheless, information for the directivity estimation is already available as a sensitivity map. The sensitivity value was taken from the amplitude of the sinusoidal signal. The x and y coordinate on the sensitivity map and the observation angle were used to calculate the sinusoid phase at a 25.4 mm distance. All signals were summed up for every observation angle (angle varied with 3° step in -80° to +80° range) and the corresponding directivity was obtained. The estimated directivity plots (circles) for the microphones are presented in Fig.13 (EMFIT-M1), Fig.14 (EMFIT-P) and Fig.15 (PVDF).

The estimated directivity was then approximated (red solid line in Fig.13-15) by a circular piston in a rigid planar baffle (RB) function [8]:

$$D_{RB}(k,a,\theta) = \frac{2J(k\cdot a\cdot\sin(\theta))}{k\cdot a\cdot\sin(\theta)}, \qquad (1)$$

where θ is the observation angle, a is microphone effective radius, k=2π/λ is wavenumber, λ=c/f is the wavelength in air, c is the ultrasound propagation velocity in air, and f is the frequency at which the directivity estimation was done.

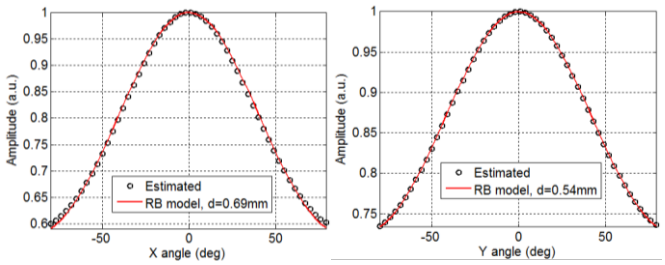

Fig. 13. Microphone EMFIT-M1 directivity along x (left) and y (right) axis.

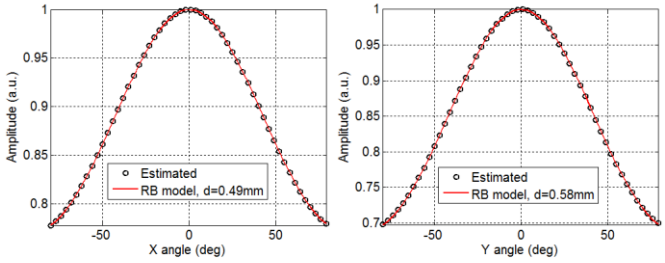

Fig. 14. Microphone EMFIT-P directivity along x (left) and y (right) axis.

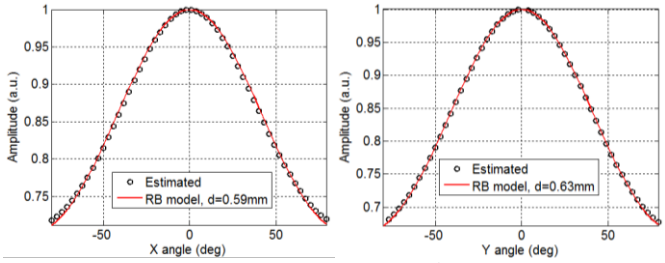

Fig. 15. Microphone PVDF directivity along x (left) and y (right) axis.

Results of the size estimation of the sensitive element for both techniques are summarized in Table II.

TABLE II
MICROPHONE SENSITIVE AREA SIZE ESTIMATION RESULTS

Estimation	-6dB sizing		Directivity fit RB model	
Microphone	*x*, mm	*y*, mm	*x*, mm	*y*, mm
EMFIT-M	0.51	0.56	0.69	0.54
EMFIT-P	0.46	0.54	0.49	0.58
PVDF	0.59	0.63	0.59	0.63

For the EMFIT-M1 microphone, the size of the sensitive element along the x axis was estimated correctly from the directivity estimation, but the -6 dB sizing (laser scan) returned a different value. It might look as though the estimated size along the x axis was smaller for the laser scan, but by looking at Fig.8 (left), one can see the reason for the underestimation was the presence of a small peak at -0.1 mm. Otherwise the element size would have been around 0.65 mm. The rest of measurements (EMFIT-M1 along y, EMFIT-P and PVDF microphones) produced matching results for both evaluation techniques.

It can be concluded, that the sensitivity map produced by laser excitation provides valuable information for the reliable estimation of the size of the sensitive element, and can replace the directivity measurement according to [64]. Furthermore, the directivity measurement requires precise beam location on the microphone tip and distance tracking. Laser scanning requires less adjustment.

C. AC Response Evaluation Using Laser Ultrasound

Thermoelastic laser generated ultrasound can also be used for microphone AC response evaluation. While the absolute measurements are complicated, the relationship between different frequency components can be obtained reliably. The laser modulation used a rectangular 4 A 100 μs duration toneburst, with a variable frequency (150-450 kHz range). The amplitude of the microphone response was extracted using SWC [56]. In order to get an integral response of the whole microphone surface, and to amplify the longitudinal wave normal to the microphone surface, a wide beam was required (comparable to the 0.5 mm diameter of the microphone sensitive area). VCSEL array laser diode was used (1.2x1 mm emitting surface, V107C021A-940 from OSRAM). The laser beam was focused onto the microphone surface using a two lens system, with a magnification of 0.5, which resulted in a beam size of 0.6x0.5 mm. The signal amplitudes at the amplifier input for 4 A laser excitation are presented in Fig.16.

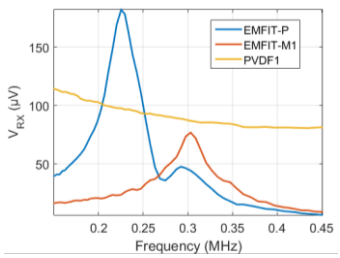

Fig. 16. Relative AC response of all microphones obtained by laser excitation.

It can be seen that the FE film (EMFIT label) and the PVDF-based microphones produced comparable output signals. The FE microphone with the thick coating (EMFIT-P) had a larger amplitude response than either the FE or the PVDF microphones coated by a thin absorber layer. It is notable, that PVDF has a much broader AC response bandwidth than FE, since its sensing element through-thickness resonance is located at 14 MHz (Table I).

The measured AC response was also used to estimate the absorbing coating thickness from the resonant frequency shift for the EMFIT material [33]. Coating material density was estimated to be 800 kg/m^3. The thin coating layer (EMFIT-M) produced a 6 % resonance frequency shift, which corresponds to a 5 μm coating thickness. The thick coating (EMFIT-P) produced a 30 % resonance shift, which corresponds to a 26 μm coating thickness.

D. AC Response Evaluation Using Reciprocity Calibration

Modification of the three-transducer reciprocity [64] sensitivity calibration was proposed in [59]. The same idea was used here to evaluate the microphone AC response. The modified technique uses a large aperture transducer, mounted on a parabolic mirror holder, and an off-axis mirror (14OAP-1-25-90-AL type from Standa Photonics) to focus the beam onto the microphone (Fig.17).

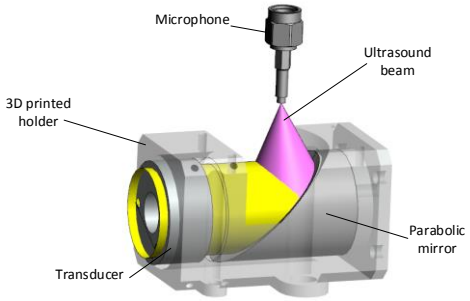

Fig. 17. Parabolic off-axis mirror focusing holder 3D drawing.

The setup involves two of the same type of transducers which are assumed to be reciprocal. The electrical transfer impedance was measured in four configurations: transducer-transducer (Z_{12}), no focusing at a distance of 25.4 mm (near field) and transducer-microphone (Z_{1M} and Z_{2M}) at a focal distance (25.4 mm):

$$Z_{12} = \frac{E_{RX2}}{I_{TX1}}, Z_{1M} = \frac{E_{RXM1}}{I_{TX1}}, Z_{2M} = \frac{E_{RXM2}}{I_{TX2}}, \quad (2)$$

where I_{TX1} and I_{TX2} are the input currents for the transmitting transducers 1 and 2 respectively, E_{RX2} is the receiving transducer 2 output voltage, E_{RXM1} and E_{RXM2} are the output voltages of the microphone, for a signal received from transducer 1 and 2 respectively.

The transducers used were designed and manufactured by the Spanish National Research Council, CSIC, and contain a 20 mm diameter piezoelectric element. More details on the transducer design can be found in [65]. With this setup, the calibration can be done in very a confined space. For comparison, the measurement distance should be 917 mm for a

20 mm diameter piezoelectric element at 300 kHz, according to [64]. It is essential, that the use of the focused source minimizes frequency-dependent diffraction effects [67]. Air attenuation and nonlinearity effects [66] are minimized, thanks to the short propagation distance and low amplitude excitation signals. The transmitting transducer was excited using the half bridge topology pulser SE-TX01-02 [69], using bipolar +/-5 V rectangular, 0.15-0.45 MHz frequency, 100 µs duration toneburst pulses. The low excitation voltage also prevented the transducer from heating and thus signal distortions. Due to the small microphone size and the acoustic impedance mismatch to air, the signals detected had low SNR, and so were averaged 1000 times. The signal received by the microphone (black line in Fig.18) was gated by selecting the part of the signal where the envelope was stable. The amplitude and phase of the received signal were estimated using the SWC technique (red line in Fig.18) [56]. The results of Fig. 18 demonstrate that at 300 kHz, the FE response is ten times higher than that of PVDF.

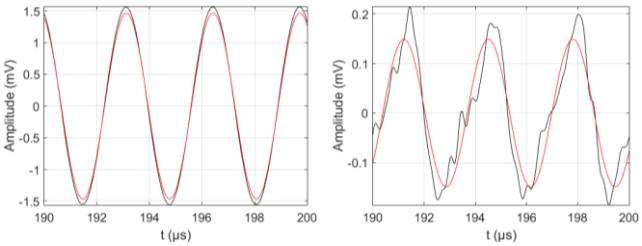

Fig. 18. Zoom-in on the signal received when excited by air-coupled transducer 300 kHz toneburst: FE (left) versus PVDF (right). Red is sinusoid with the amplitude and phase extracted using SWC, black is raw signal.

The reception sensitivity of the microphone is [59]:

$$M_M = \sqrt{\frac{2G_{TT}c \cdot d^2 Z_{1M} Z_{2M}}{A\rho f^2 Z_{12}}}, \quad (3)$$

where G_{TT} is the diffraction correction factor for transducer-transducer propagation (obtained using the paraxial expansion described in [28]), ρ is the air density, A is the active surface area of the transducer, and d is the propagation distance.

Ultrasound attenuation in air was not accounted for, due to the short propagation distances. The expected focal spot size at 300 kHz is 1.7 mm, and the microphone's sensitive element diameter is 0.5 mm, and therefore beam size correction was not necessary.

The results for all microphone measurements are presented in Fig.19.

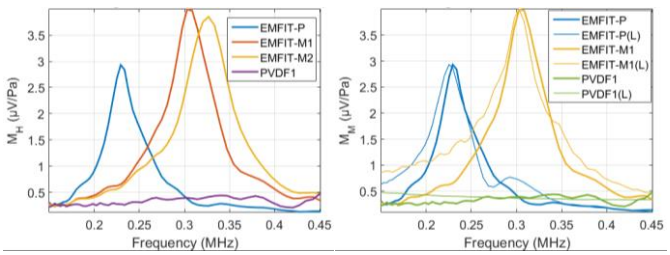

Fig. 19. Microphone AC response obtained by three transducer reciprocity calibration (left) comparison to laser excitation (right).

The laser measurement results (Fig.19 right, thin lines (L)) have been added for comparison with amplitude, and are normalized to match the calibration results. It can be concluded that both laser excitation and reciprocity calibration produced similar AC responses. Laser excitation is not affected by air movement or air temperature influence on the propagation time.

The FE-based microphone has much better sensitivity at its first through thickness resonant frequency, compared to its PVDF-based counterpart. Performance beyond this resonance is comparable, for the case where a thin light-absorbing coating is used. A thick coating lowers the resonance frequency as expected, and results in the sensitivity and bandwidth being reduced.

Due to the large impedance mismatch between the air and any solid material (in this case with PVDF and FF), the active film response is quite resonant (much more resonant than what can be observed in the case of hydrophones in water). The location of the thickness resonance depends on the ultrasonic velocity in the film, the film thickness and any additional load added to the film. It must be taken into account that both density and elastic constant of FF are very low, so the FF thickness resonance is very sensitive to any mass load added. The expected resonance of the FF film is about 320 kHz, which correspond well with results from EMFIT-M1. EMFIT-P shows a resonance displaced to lower frequency (230 kHz), due to the additional mass of the thick coating added to the FF film. Precise and thin layer coating control, from spin-coating, sputtering or vacuum evaporation, can reduce this frequency drop compared to the uncoated device. However, it should be remembered that no coating would be required if there was no need to provide absorption of the incident laser beam. In the case of the PVDF sensor, the thickness resonance is expected to appear at 14 MHz (Table I), because the ultrasonic compression wave velocity in the PVDF is larger and its thickness is smaller, and therefore the PVDF response is quite flat. PVDF is also more dense, so the additional coating used does not influence the frequency shift as much as for FE.

IV. Conclusion

It was demonstrated that a miniature, 0.5 mm diameter microphone can be produced using the FE film. Production is simple and involves adhesively bonding the FE film on the end of the semirigid coaxial cable.

Another contribution proposed in the paper is the sensitivity map measurement technique, which uses thermoelastic mode laser excitation. Excitation was accomplished by focusing the edge-emitting laser diode on microphone surface, attaining 60 µm resolution of the sensitivity map image. Defocusing and astigmatism were exploited usefully for laser beam profile symmetrization, resulting in very simple lens system. The whole laser excitation system design is very compact, being 40x40 mm in size. It was demonstrated that the microphone has a sensitive area diameter slightly wider than electrode diameter of 0.5 mm, which was also confirmed by estimating the microphone directivity from the sensitivity map. The estimated directivity matches the *Jinc* function, corresponding to a

circular piston in a rigid planar baffle.

The absolute sensitivity and AC response was obtained by a three transducer reciprocity calibration technique. The sensitivity measurement demonstrated that the FE microphone peak sensitivity is 4 μV/Pa, which is much higher than for the microphone made of PVDF. The sensitivity can be further enhanced, as the current device used FE materials with d_{33}=80 pC/N, but newer FE materials have d_{33}=1400 pC/N [35]. Broader bandwidth and higher sensitivity can be achieved if such materials appear on the market.

One more novelty presented here is the microphone relative AC response measurement, using laser ultrasound. A medium power VCSEL array laser diode was used for thermoelastic excitation of the whole microphone surface.

ACKNOWLEDGMENT

Authors acknowledge the help of A. Aleksandrovas and M. Varatinskas in experimental modules preparation.

REFERENCES

[1] "1/8-inch Pressure-field Microphone Type 4138," Brüel & Kjær, 2021.

[2] R. J. Kazys, R. Sliteris, and J. Sestoke, "Air-Coupled Low Frequency Ultrasonic Transducers and Arrays with PMN-32%PT Piezoelectric Crystals," *Sensors*, vol.17, no.1., pp. 1-20, Jan 2017. DOI:10.3390/s17010095

[3] G. Benny, G. Hayward, "Beam Profile Measurements and Simulations for Air-Coupled Ultrasonic Transducers," In *Proc. IEEE IUS*, vol. 1-2, pp.1041-1044, 1999.

[4] G. Benny, G. Hayward, and R. Chapman, "Beam profile measurements and simulations for ultrasonic transducers operating in air," *J. Acoust. Soc. Amer*., vol. 107, no. 4, pp. 2089–2100, 2000. DOI:10.1121/1.428491

[5] G. Allevato, J. Hinrichs, M. Rutsch, J.P. Adler, A. Jager, M. Pesavento, M. Kupnik, "Real-Time 3-D Imaging Using an Air-Coupled Ultrasonic Phased-Array," *IEEE Trans. Ultrason. Ferroelect. Freq. Control*, vol. 68, no. 3, pp.796-806, Mar 2021. DOI:10.1109/TUFFC.2020.3005292

[6] *Non-destructive testing - Characterization and verification of ultrasonic examination equipment - Part 2: Probes*, EN 12668-2:2010, 2010.

[7] K.A. Wear, Y.B. Liu, "Considerations for Choosing Sensitive Element Size for Needle and Fiber-Optic Hydrophones-Part II: Experimental Validation of Spatial Averaging Model," *IEEE Trans. Ultrason. Ferroelect. Freq. Control*, vol.66, no. 2, pp.340-347, Feb 2019. DOI:10.1109/TUFFC.2018.2886071

[8] K.A. Wear, C. Baker, P. Miloro, "Directivity and Frequency-Dependent Effective Sensitive Element Size of Needle Hydrophones: Predictions From Four Theoretical Forms Compared With Measurements," *IEEE Trans. Ultrason. Ferroelect. Freq. Control*, vol.65, no.10, pp.1781-1788, OCT 2018. DOI:10.1109/TUFFC.2018.2855967

[9] K.A. Wear, S.M. Howard, "Directivity and Frequency-Dependent Effective Sensitive Element Size of a Reflectance-Based Fiber-Optic Hydrophone: Predictions From Theoretical Models Compared With Measurements," *IEEE Trans. Ultrason. Ferroelect. Freq. Control*, vol.65, no. 12, pp. 2343-2348, Dec 2018. DOI:10.1109/TUFFC.2018.2872840

[10] S.J. Sanabria, T. Marhenke, R. Furrer, J. Neuenschwander, "Calculation of Volumetric Sound Field of Pulsed Air-Coupled Ultrasound Transducers Based on Single-Plane Measurements," *IEEE Trans. Ultrason. Ferroelect. Freq. Control*, vol. 65, no.1, pp.72-84, Jan 2018. DOI:10.1109/TUFFC.2017.2773619.

[11] W. Cui, R. N. Miles, Q. Su, "A Robust Miniature Silicon Microphone Diaphragm," Sensors & Transducers Journal, vol.7, pp. 63-77, Oct 2009.

[12] W. Galhraith, G. Hayward, "Development of a PVDF membrane hydrophone for use in air-coupled ultrasonic transducer calibration", *IEEE Trans. Ultrason. Ferroelect. Freq. Control*, vol. 45, no.6. pp.1549-1558, (1998). DOI:10.1109/58.738294.

[13] A.G. Bashford, D.W. Schindel, D.A. Hutchins, W.M.D. Wright, "Field characterization of an air-coupled micromachined ultrasonic capacitance transducer," *J. Acoust. Soc. Am.*, vol.101, no.1 , pp.315-322, Jan 1997. DOI:10.1121/1.418011.

[14] W. Westerveld, "Silicon photonic micro-ring resonators to sense strain and ultrasound," Ph.D. thesis, Delft University of Technology, Faculty Applied Sciences, Department of Imaging Physics, 2014.

[15] K. Chen, Z. F. Gong, M. Guo, S.C. Yu, C. Qu, X. L. Zhou, Q. X. Yu, "Fiber-optic Fabry-Perot interferometer based high sensitive cantilever microphone," *Sens. Actuator A Phys*., vol.279, pp.107-112, Aug 2018. DOI:10.1016/j.sna.2018.06.010

[16] S.L. Liao, T. Wong, Z. Wang, R. Wang, E. Clutter, H.T. Chien, "Miniature Fiber Laser Microphones with Graphene Diaphragms," *In Proc. IEEE RAPID*, pp. 197-200, 2018.

[17] "Fibre-optic Hydrophone Systems (FOHS) v2," Precision Acoustics, 2022.

[18] W.Rohringer, T.Heine, R.Sommerhuber, N.Lehmann, B. Fischer, "Optical Microphone as Laser-Ultrasound Detector," *In Proc. DAGA*, pp.1-4, 2018.

[19] J.C. Grager, D. Kotschate, J. Gamper, M. Gaal, K. Pinkert, H. Mooshofer, M. Goldammer, Ch. U. Grosse, "Advances in air-coupled ultrasonic testing combining an optical microphone with novel transmitter concepts," *In Proc. ECNDT*, pp. 1-10, 2018.

[20] M. Almqvist, A. Holm, H.W. Persson, K. Lindstrom, "Characterization of air-coupled ultrasound transducers in the frequency range 40 kHz-2 MHz using light diffraction tomography," *Ultrasonics*, vol.37, no.8, pp.565-575, Jan 2000. DOI:10.1016/S0041-624X(99)00168-7.

[21] R.A. Noble, T.J. Robertson, J.S. McIntosh, D.A. Hutchins, D.R. Billson, "A novel coupled piezoelectric micromachined ultrasonic transducer based on piston mode," *IEEE Trans. Ultrason. Ferroelect. Freq. Control*, vol. 68, no. 11, pp. 3396- 3405, Nov 2021. DOI:10.1109/TUFFC.2021.3090043

[22] A. Neild, D.A. Hutchins, T.J. Robertson, L.A.J. Davis, D.R. Billson, "The radiated fields of focussing air-coupled ultrasonic phased arrays," *Ultrasonics*, vol. 43, no. 3, pp.183-195, Jan 2005. DOI:10.1016/j.ultras.2004.04.006.

[23] S.A. Zawawi, A.A. Hamzah, B.Y. Majlis, F. Mohd-Yasin, "A Review of MEMS Capacitive Microphones," *Micromachines*, vol.11, no.5, 484, May 2020. DOI:10.3390/mi11050484

[24] T. Ling, S.L. Chen, L.J. Guo, "High-sensitivity and wide-directivity ultrasound detection using high Q polymer microring resonators," *Appl. Phys. Lett*., vol.98, no. 20, 204103, May 2011. DOI:10.1063/1.3589971.

[25] S.D. Wang, Y.C. Chen, S.C. Lo, Y.J. Wang, M.C. Wu, W.L. Fang, "On The Performance Enhancement of Cantilever Diaphragm Piezoelectric Microphone," *IEEE Sensors*, 2021. DOI:10.1109/SENSORS47087.2021.9639769.

[26] S. Basiri-Esfahani, A. Armin, S. Forstner, W.P. Bowen, "Precision ultrasound sensing on a chip," *Nat. Commun*. vol.10, 132, Jan 2019. DOI:10.1038/s41467-018-08038-4.

[27] G. Caliano, V. Foglietti, E. Cianci and M. Pappalardo, "A silicon microfabricated electrostatic transducer:1 MHz transmission in air and in water," *Microelectron. Eng*., vol. 53, no,1-4, 573-576, pp. Jun 2000. DOI:10.1016/S0167-9317(00)00381-6.

[28] S.J. Rupitsch, R. Lerch, J. Strobel, A. Streicher, "Ultrasound Transducers Based on Ferroelectret Materials," *IEEE Trans. Dielectr. Electr. Insul*., vol.18, no.1, pp.69-80, Feb 2011. DOI:10.1109/TDEI.2011.5704495.

[29] J.L. Ealo, F. Seco, and A.R. Jimenez, "Broadband EMFi-Based Transducers for Ultrasonic Air Applications," *IEEE Trans. Ultrason. Ferroelect. Freq. Control*, vol.55, no.4 , pp.919-929, Apr 2008. DOI:10.1109/TUFFC.2008.727.

[30] I. Graz, M. Kaltenbrunner, C. Keplinger, R. Schwodiauer, S. Bauer, S.P. Lacour, S. Wagner, "Flexible ferroelectret field-effect transistor for large-area sensor skins and microphones," *Appl. Phys. Lett*, vol.89, no. 7, 073501, Aug 2006. DOI:10.1063/1.2335838

[31] V. Bovtun, J. Doring, J. Bartusch, U.Beck, A. Erhard, Y. Yakymenko, "EMFIT Ferroelectret Film Transducers for Non-Contact Ultrasonic Testing," *In Proc. ECNDT*, 2006.

[32] J.Q. Aguilar, M. Munoz, T.G. Alvarez-Arenas, "Interpretation of the Thickness Resonances in Ferroelectret Films Based on a Layered Sandwich Mesostructure and a Cellular Microstructure," *IEEE Trans. Ultrason. Ferroelect. Freq. Control*, vol.68, no.4, pp.1245-1252, Apr 2021. DOI:10.1109/TUFFC.2020.3025358

[33] J. Quirce, L. Svilainis, J. Camacho, T.G. Alvarez-Arenas, "Ferroelectret Ultrasonic Transducers for Pulse-Echo Water Immersion," *Appl. Sci*., vol. 10, no. 24, 8771, Dec 2020. DOI:10.3390/app10248771

[34] J. Hillenbrand and G. M. Sessler, "DC-biased ferroelectrets with large piezoelectric d33-coefficients," *J. Appl. Phys*., vol. 103, no. 7, p. 074103, 2008.

[35] X. Zhang, J. Hillenbrand, G.M. Sessler, "Improvement of piezoelectric activity of cellular polymers using a double-expansion process," J. Phys. D., vol.37, no.15, pp.2146-2150, Aug 2004. DOI:10.1088/0022-3727/37/15/015

[36] J. Hillenbrand and G. Sessler, "High-sensitivity piezoelectric microphones based on stacked cellular polymers films," *J. Acoust. Soc. Amer*., vol. 116, pp. 3267–3270, 2004. DOI:10.1121/1.1810272

[37] J. Hillenbrand, G.M. Sessler, "Piezoelectret microphones with high sensitivity," *In Proc. ISE*, pp.125-128, 2005.

[38] V. Bovtun, J. Doring, M. Wegener, J. Bartusch, U. Beck, A. Erhard, V. Borisov, "Air-Coupled Ultrasonic Applications of Ferroelectrets," *Ferroelectrics*, vol.370, pp.11-17, PII 905071006, 2008. DOI:10.1080/00150190802380243

[39] "Ultrasonic Applications for Knowles Electret and MEMS Microphones," Application Note 17, Knowles Electronics, 2013.

[40] T. E. G. Alvarez-Arenas, H. Calas, J. E. Cuello, A. R. Fernandez, M. Munoz, "Noncontact ultrasonic spectroscopy applied to the study of polypropylene ferroelectrets," *J. Appl. Phys*, vol.108, no.7, 074110, Oct 2010. DOI:10.1063/1.3490788

[41] L. Svilainis, V. Dumbrava, D. Kybartas, "Evaluation of the ultrasonic preamplifier noise voltage density," *J. Circuits, Syst. Comput*., vol.23, no.1, 1450007, Jan 2014. DOI:10.1142/S0218126614500078

[42] L.Svilainis, D.Kybartas, A.Aleksandrovas, T.E.G Alvarez-Arenas,. "High frequency focused imaging for ultrasonic probe integrity inspection," *NDT E Int*., vol.116, 2020, 102360. DOI: 10.1016/j.ndteint.2020.102360

[43] L. Svilainis, A. Chaziachmetovas, D. Kybartas, T.G. Alvarez-Arenas, "Air-Coupled Ultrasonic Probe Integrity Test Using a Focused Transducer with Similar Frequency and Limited Aperture for Contrast Enhancement," *Sensors*, vol.20, no.24, 7196, Dec 2020. DOI:10.3390/s20247196

[44] J. P. Monchalin, "Laser-Ultrasonics: Principles And Industrial Applications", *e-Journal of Nondestructive Testing*, vol. 3, pp.1-43, 2020.

[45] S. Dixon, T. Harrison, Y. Fan, P. A. Petcher, "Thermoelastic laser generated ultrasound using a ring source," *J. Phys. D: Appl. Phys*., vol. 45, no.17, 175103, May 2012. DOI: 10.1088/0022-3727/45/17/175103

[46] L. F. Bresse, D. A. Hutchins, "Transient generation by a wide thermoelastic source at a solid surface," *J. Appl. Phys*., vol. 65, pp.1441-1449, 1989. DOI: 10.1063/1.342956

[47] C. B.Scruby, H. N. G.Wadley, R. J. Dewhurst, S. B. Palmer, D. A. Hutchins, "A laser-generated standard acoustic emission source," *Mater. Eval*., vol. 39, pp. 1250-1254, Dec. 1981.

[48] L. Svilainis, A. Chaziachmetovas, V. Eidukynas, A. Aleksandrovas, M. Varatinskas, "Compact Laser Driver for Ultrasonic Arbitrary Position and Width Pulse Sequences Generation," *IEEE Trans. Instrum. Meas*., vol.70, 7006815, 2021. DOI:10.1109/TIM.2021.3120144

[49] V. V. Krylov, "Directivity patterns of laser-generated sound in solids: Effects of optical and thermal parameters," *Ultrasonics*, vol. 69, Jul 2016. pp. 279–284. DOI:10.1016/j.ultras.2016.01.011

[50] F. Gao, R. Kishor, X. Feng, S. Liu, R. Ding, R. Zhang, Y. Zheng, "An analytical study of photoacoustic and thermoacoustic generation efficiency towards contrast agent and film design optimization," *Photoacoustics*, vol. 7, pp. 1–11, Sep 2017. DOI:10.1016/j.pacs.2017.05.001

[51] M.N. Hasan, M.U. Haque, Y.C. Lee, "Deastigmatism, circularization, and focusing of a laser diode beam using a single biconvex microlens," *Opt. Eng*., vol.55, no.9, 095107, Sep 2016. DOI:10.1117/1.OE.55.9.095107

[52] M. Serkan, H. Kirkici, "Reshaping of a Divergent Elliptical Gaussian Laser Beam Into a Circular, Collimated, and Uniform Beam With Aspherical Lens Design," *IEEE Sens. J.*, vol.9, no.1-2, pp.36-44, Jan-Feb 2009. DOI:10.1109/JSEN.2008.2008882

[53] X.Q. Zhou, B.K.A. Ngoi, S.S. Koh, "Single aspherical lens for deastigmatism, collimation, and circularization of a laser beam," *Appl. Opt.*, vol.39, no.7, pp.1148-1151, Mar 2000.

[54] M. Erfanzadeh, P.D. Kumavor, Q. Zhu, "Laser scanning laser diode photoacoustic microscopy system," *Photoacoustics*, vol. 9, pp. 1-9, MAR 2018. DOI:10.1016/j.pacs.2017.10.001

[55] A. Hariri, A. Fatima, N. Mohammadian, S. Mahmoodkalayeh, M.A. Ansari, N. Bely, M.R.N. Avanaki, "Development of low-cost photoacoustic imaging systems using very low-energy pulsed laser diodes," *J. Biomed. Opt*., vol.22, no. 7, 075001, JUL 2017. DOI: 10.1117/1.JBO.22.7.075001

[56] V. Dumbrava, L. Svilainis, "The automated complex impedance measurement system," *Elektron. Elektrotech*., vol.76, no.4., pp.59-62, 2007.

[57] L. Svilainis, V. Dumbrava, S. Kitov, A. Aleksandrovas, P. Tervydis, D. Liaukonis, Electronics for Ultrasonic Imaging System, *Elektron. Elektrotech*., vol. 20, no. 7, pp. 51-56, 2014. DOI: 10.5755/j01.eee.20.7.8024.

[58] Y.B. Wang, M. Sun, Y.G. Cao, J. Zhu, "Application of optical interferometry in focused acoustic field measurement," *J. Sound Vib*., vol.426, pp.234-243, Jul 2018. DOI:10.1016/j.jsv.2018.04.023

[59] L. Svilainis, A. Chaziachmetovas, T. E. G. Alvarez-Arenas, "Ultrasonic needle hydrophone calibration in air by parabolic off-axis mirror focused beam using three-transducer reciprocity," unpublished.

[60] D. A.Hutchins, R. J. Dewhurst, S. B.Palmer, "Laser generated ultrasound at modified metal surfaces," *Ultrasonics*, vol.19, no.103, pp. 103-108, May 1981. DOI:10.1016/0041-624X(81)90078-0

[61] C. Edwards, T. Stratoudaki and S. B. Palmer "A New Thermoelastic Source Model for Non-Metals," *In Proc. RPQNE*, Vol. 22, pp. 326-332, 2003.

[62] J.J. Wang, B.Q. Xu, Z.H. Shen, X.W. Ni, J. Lu, "Influence of transparent coating thickness on thermoelastic force source and laser-generated ultrasound waves," *Appl. Surf. Sci*., vol.255, no. 16, pp. 7172-7178, May 2009. DOI: 10.1016/j.apsusc.2009.03.054

[63] F. Gao, R. Kishor, X. Feng, S. Liu, R.Ding, R. Zhang, Y. Zheng "An analytical study of photoacoustic and thermoacoustic generation efficiency towards contrast agent and film design optimization," *Photoacoustics*, vol.7, 2017, pp. 1–11. DOI:10.1016/j.pacs.2017.05.001

[64] *Ultrasonics - Hydrophones - Part 3: Properties of hydrophones for ultrasonic fields up to 40 MHz*, IEC 62127-3:2007, 2007.

[65] T.E.G. Alvarez-Arenas, "Air-Coupled Piezoelectric Transducers with Active Polypropylene Foam Matching Layers," *Sensors*, vol. 13, no.5, pp. 5996-6013, 2013. DOI: 10.3390/s130505996.

[66] L. Gaete-Garreton, J. A. Gallego-Juárez, E. Riera, "Nonlinear problems in the generation, propagation and measurement of high intensity ultrasonic waves in air," *In: Proc. Mtgs. Acoust*. Vol.32, 045027, 2017. DOI: 10.1121/2.0000782.

[67] A. Selfridge, P. A. Lewin, "Wideband spherically focused PVDF acoustic sources for calibration of ultrasound hydrophone probes," *IEEE Trans. Ultrason. Ferroelect. Freq. Control*, vol.47, no.6, pp. 1372-1376, 2000. DOI: 10.1109/58.883526.

[68] *Underwater acoustics - Hydrophones - Calibration of hydrophones - Part 1: Procedures for free-field calibration of hydrophones*. IEC 60565-1:2020. International Electrotechnical Commission, 2020.

[69] L. Svilainis, A. Chaziachmetovas, V. Dumbrava, "Half bridge topology 500 V pulser for ultrasonic transducer excitation," *Ultrasonics*, vol.59, pp. 79-85, 2015. DOI: 10.1016/j.ultras.2015.01.014.

[70] T.D. Mast, F. Yu, "Simplified expansions for radiation from a baffled circular piston," *J. Acoust. Soc. Amer*., vol.118, np.6, pp.3457-3464, 2005. DOI: 10.1121/1.2108997.

[71] D.A. Hutchins, T.J. Robertson, D.R. Billson, "New designs of focused air-coupled ultrasonic transducer," *Revista de Acustica*, vol.33, pp. 3-4, 2002.

[72] T.E.G. Alvarez-Arenas, J. Camacho, C. Fritsch, "Passive focusing techniques for piezoelectric air-coupled ultrasonic transducers," *Ultrasonics*, vol.67, pp.85-93, 2016. DOI: 10.1016/j.ultras.2016.01.001.